Ability of the land surface model ISBA-A-gs to simulate leaf area index at the global scale: Comparison with satellites products

Anne-Laure Gibelin, Jean-Christophe Calvet, Jean-Louis Roujean, Lionel Jarlan, S. Los

Ability of the land surface model ISBA-A-gs to simulate leaf area index at the global scale: Comparison with satellites products

Anne-Laure Gibelin,[1] Jean-Christophe Calvet,[1] Jean-Louis Roujean,[1] Lionel Jarlan,[1] and Sietse O. Los[2]

Received 20 September 2005; revised 26 January 2006; accepted 13 June 2006; published 19 September 2006.

[1] The land surface model (LSM) ISBA-A-gs (Interactions between Soil, Biosphere and Atmosphere, CO_2-reactive) is specifically designed to simulate leaf stomatal conductance and leaf area index (LAI) in response to climate, soil properties, and atmospheric carbon dioxide concentration. The model is run at the global scale, forced by the GSWP-2 meteorological data at a resolution of 1° for the period of 1986–1995. We test the model by comparing the simulated LAI values against three satellite-derived data sets (ISLSCP Initiative II data, MODIS data and ECOCLIMAP data) and find that the model reproduces the major patterns of spatial and temporal variability in global vegetation. As a result, the mean of the maximum annual LAI estimates of the model falls within the range of the various satellite data sets. Despite no explicit representation of phenology, the model captures the seasonal cycle in LAI well and shows realistic variations in start of the growing season as a function of latitude. The interannual variability is also well reported for numerous regions of the world, particularly where precipitation controls photosynthesis. The comparison also reveals that some processes need to be improved or introduced in the model, in particular the snow dynamics and the treatment of vegetation in cultivated areas, respectively. The overall comparisons demonstrate the potential of ISBA-A-gs model to simulate LAI in a realistic fashion at the global scale.

Citation: Gibelin, A.-L., J.-C. Calvet, J.-L. Roujean, L. Jarlan, and S. O. Los (2006), Ability of the land surface model ISBA-A-gs to simulate leaf area index at the global scale: Comparison with satellites products, *J. Geophys. Res.*, *111*, D18102, doi:10.1029/2005JD006691.

1. Introduction

[2] Climate and vegetation interact with each other at various temporal and spatial scales. Climate influences the vegetation growth, essentially through solar radiation, air temperature and precipitation. Vegetation modulates the surface fluxes of heat, moisture and momentum (see a review by *Pielke et al.* [1998]) from the land surface to the atmosphere. The atmospheric carbon dioxide (CO_2) concentration is also involved in these interactions. First, CO_2 is a greenhouse gas and its rising concentration in the atmosphere is projected to cause an increase in surface temperatures of 1.4 to 5.8°C by the end of the 21st century [*Houghton et al.*, 2001]. Second, increased CO_2 levels are likely to cause an increase in water use efficiency [*Körner*, 2000, 2003]. Finally, the terrestrial biosphere plays an important role in absorbing and releasing large amounts of CO_2 during the year: during the past decades the terrestrial biosphere has been a net sink for atmospheric CO_2 [*Keeling et al.*, 1996; *Ciais et al.*, 1995], but some models indicate that the biosphere may become a source if CO_2 levels continue to rise [*Cox et al.*, 2000]. Uncertainties in estimates of carbon fluxes at a global scale as well as their evolution are still high [*Houghton et al.*, 2001], and the processes responsible for their evolution are insufficiently well understood and need to be better explored.

[3] The investigation of the land surface-atmosphere interactions at decadal or century timescales is effectively addressed by numerical modeling experiments. Soil-vegetation-atmosphere transfer (SVAT) schemes are designed to simulate exchanges of energy, matter and momentum between the land surface and the atmosphere. From simple bulk parameterizations in the 1970s, they have evolved into sophisticated land surface models (LSMs), including numerous geophysical and biogeochemical processes [*Pitman*, 2003; *Sellers et al.*, 1997]. The new generation LSMs include interactive vegetation and allow simulating the exchanges of carbon at the canopy level and the vegetation growth [e.g., *Krinner et al.*, 2005; *Calvet et al.*, 1998; *Cox et al.*, 1998; *Dickinson et al.*, 1998; *Foley et al.*, 1996; *Sellers et al.*, 1996a]. Other models, designed for ecological studies, simulate carbon exchanges between the terrestrial biosphere and the atmosphere (see the review by *Arora* [2002] of the processes of the vegetation dynamics and of the different models in which they are implemented). In this study, we focus on SVAT-type LSMs that are able to provide continental boundary conditions needed by atmo-

[1]Groupe d'Etude de l'Atmosphère Météorologique, Météo-France/Centre National de Recherches Météorologiques, Toulouse, France.
[2]Department of Geography, University of Wales, Swansea, UK.

0148-0227/06/2005JD006691

spheric models. Two main vegetation properties drive the water and CO_2 exchanges between vegetation and the atmosphere in such LSMs: the leaf stomatal conductance (g_s) and the leaf area index (LAI). Both g_s and LAI depend on environmental factors, principally climate and atmospheric CO_2 concentration. They are foreseen to be impacted by global change [*Körner*, 2000, 2003] and in turn to modify climate over vegetated regions. Several modeling studies have addressed the magnitude of feedback effects of vegetation on climate under a doubled atmospheric CO_2 concentration [e.g., *Douville et al.*, 2000; *Bounoua et al.*, 1999; *Betts et al.*, 1997; *Sellers et al.*, 1996b].

[4] LAI is a critical parameter of the LSMs. In particular, realistic LAI are required to simulate realistic surface fluxes in LSMs. LAI is still often a prescribed parameter when the LSM is used in an atmospheric model [*Arora*, 2002]. In this case, global LAI maps are derived from remote sensing data or from land cover classifications and look-up table. Satellite observations are the only means to provide spatially and temporally varying LAI fields on a routine basis on regional and global scales. Different methods exist to estimate LAI from space, ranging from a dynamic scaling of vegetation indices to advanced modeling with radiative transfer codes. LAI maps are usually monthly climatologies as satellite data are available only for a limited period (since 1980s up to now). Alternatively, LAI can now be calculated dynamically by the new generation LSMs. This allows simulating coherent spatial and temporal variability of vegetation, as well as assessing the response of vegetation to changes in environmental factors. This study is an attempt to validate the global distribution of LAI simulated by the ISBA-A-gs LSM [*Calvet et al.*, 1998] through a comparison with satellite data. Until now, the model has only been evaluated at the local scale.

[5] The aim of this paper is (1) to describe the implementation at the global scale of the new generation land surface model ISBA-A-gs and (2) to validate the simulated LAI by using three satellite-derived data sets (ISLSCP-II [*Los et al.*, 2000], MODIS [*Myneni et al.*, 2002] and ECOCLIMAP [*Masson et al.*, 2003]). The data sets are described in section 2. Section 3 presents the ISBA-A-gs model, the assignment of biome-dependent parameters in the model, and the experimental design of the global simulations. The mean and the interannual variability of simulated LAI are both compared with the satellite data (section 4). Finally, in section 5 we summarize the results and indicate future directions for research work in the area. Details of the model are discussed in Appendices A, B, and C.

2. Presentation of the Data Sets

2.1. GSWP-2

[6] The Global Soil Wetness Project (GSWP; http://www.iges.org/gswp/) is an environmental modeling research activity of the Global Land-Atmosphere System Study (GLASS) and the International Satellite Land-Surface Climatology Project (ISLSCP), both contributing projects of the Global Energy and Water Cycle Experiment (GEWEX) [*Dirmeyer et al.*, 1999, 2002, 2005]. One of its main goals is to produce state-of-the-art global data sets of land surface fluxes, state variables of the continental surfaces, and related hydrologic quantities.

[7] The GSWP-2 meteorological data set provide forcing data for climate models at the global scale. A comprehensive data set of near-surface atmospheric variables is available from July 1982 to December 1995, at 3-hour intervals, and at $1 \times 1^\circ$ resolution. For the current study we used air temperature at 2 m, air specific humidity at 2 m, wind speed at 10 m, surface incident shortwave radiation, surface incident longwave radiation, surface pressure, rainfall and snowfall rates. Several atmospheric forcing data sets were provided in the framework of GSWP-2, for running different sensitivity experiments [*Zhao and Dirmeyer*, 2003]. The data set selected for the baseline simulation is based on the National Centers for Environmental Prediction/Department of Energy (NCEP/DOE) reanalysis. Air temperature and air specific humidity are hybridized with CRU (Climatic Research Unit) data. Precipitation data result from a combination of gauge-based (CRU from July 1982 to December 1985 and Global Precipitation Climatology Center (GPCC) from January 1986 to December 1995) and satellite-based (Global Precipitation Climatology Project, GPCP) products depending on the gauge density. A wind correction is applied to correct for the gauge undercatch. Since NCEP reanalysis overestimates the wind speed, the quality of the precipitation of the baseline simulation is poor over Europe [*Decharme and Douville*, 2005; *Tanaka et al.*, 2004]. Therefore we preferred using the NCEP reanalysis, hybridized with CRU and GPCC gauge-based data for precipitation, corresponding to the P3 sensitivity experiment in GSWP-2. The European Center for Medium-range Weather Forecast (ECMWF) reanalysis presently yields an a priori better data set [*Tanaka et al.*, 2004], but it was not available at the time of this study for all the GSWP-2 simulation period.

2.2. ECOCLIMAP

[8] ECOCLIMAP is a global surface parameter database at a 1-km resolution [*Masson et al.*, 2003] (http://www.cnrm.meteo.fr/gmme/PROJETS/ECOCLIMAP/page_ecoclimap.htm). It provides a coherent ensemble of key surface parameters necessary to initialize the LSMs at a wide range of horizontal scales (among which soil texture, albedo, emissivity, surface roughness and LAI). It uses a "tile" approach and includes 15 different surface types: bare soil, rocks, permanent snow and ice, deciduous broadleaf trees, evergreen broadleaf trees, needleleaf trees, C_3 crops, C_4 crops, irrigated crops, C_3 natural herbaceous vegetation, C_4 natural herbaceous vegetation, wetland herbaceous vegetation or irrigated grasslands, sea, inland water bodies and urbanized areas. In ECOCLIMAP, the strategy for mapping surface parameters is achieved in two steps. First, a land cover classification is built to segregate pixel values that are closely responsive in terms of spectral and temporal behaviors. Second, on the basis of the classification nomenclature, look-up tables (LUTs) allow assigning similar values of surface parameters to each pixel of a same class. In this way, surface products are spatially consistent and temporally coherent, as required in meteorology. For LAI, the first version, ECOCLIMAP-I, relies on the analysis of time series of the Normalized Difference Vegetation Index (NDVI) from AVHRR sensor. The yearly evolution of LAI is scaled between the minimum and maximum values of the seasonal NDVI. Interannual variability of

LAI is not addressed. The global LAI data set was validated through a comparison with in situ measurements and with satellite-derived global data sets [*Masson et al.*, 2003].

[9] In this study, ECOCLIMAP is used in a twofold way: (1) It provides the input surface parameters required by ISBA-A-gs (except LAI, which is a prognostic variable of the model and not a prescribed parameter, and vegetation fraction and roughness length, which are calculated by ISBA-A-gs according to the LAI value) and (2) the ECOCLIMAP LAI is used for the validation of the model results.

2.3. ISLSCP-Initiative II

[10] The International Satellite Land-Surface Climatology Project (ISLSCP; http://www.gewex.org/islscp.html) initiative II has a remit from GEWEX to produce a consistent collection of high-priority global data sets using existing data sources and algorithms, designed to satisfy the users needs [*Hall et al.*, 2005]. The global data sets are mapped at consistent spatial and temporal resolutions and are organized along seven themes: Carbon, Hydrology, Near-surface meteorology, Radiation, Snow, Socioeconomic and Vegetation. The data sets span the 10-year period, 1986–1995.

[11] Biophysical parameters are derived from the FASIR-NDVI (Fourier Adjusted, Solar zenith angle correction, Interpolation, and Reconstruction of NDVI) product [*Los et al.*, 2000, 2005]. The green and total LAI are calculated from AVHRR NDVI values by using appropriate relationships between the LAI, the fraction of photosynthetically active radiation (FPAR) absorbed by the vegetation, and NDVI. The satellite data are simultaneously corrected for sensor degradation, volcanic aerosol effects, cloud contamination, short-term atmospheric effects, solar zenith angle and view zenith angle variations, and missing data [*Los et al.*, 2000, 2005].

[12] In the GSWP-2 project, the characteristics of the land surface are mostly specified from soil and vegetation data of ISLSCP Initiative II. In particular, the LAI data set is available at a monthly time step, at a $1 \times 1^\circ$ resolution for the period 1982–1995. In this study, we used an extended green LAI data set of ISLSCP available for 1982–1998, with a 10-day time step [*Los et al.*, 2000], for the validation of the LAI simulated by ISBA-A-gs. This enhanced temporal resolution allowed us to estimate the start of the growing season. This LAI data set is referred to as ISLSCP-II in the remainder of the paper.

2.4. MODIS

[13] The Moderate Resolution Imaging Spectroradiometer (MODIS; http://modis.gsfc.nasa.gov/) is an instrument on board NASA's Terra and Aqua platforms for remote sensing of the Earth atmosphere, oceans and land surface. The MODIS LAI and FPAR Level 4 products are globally tiled and are projected on a sinusoidal grid, which is an equivalent projection conserving the surface areas. They are produced daily at 1 km spatial resolution (MOD15A1) and composited over an 8-day period on the basis of the maximum FPAR value [*Justice et al.*, 2002; *Myneni et al.*, 2002]. Collection 4 is the latest version of Terra MODIS products and consists of the entire time series, starting from February 2000 to the present. The Collection 4 MODIS LAI/FPAR operational algorithm utilizes the MODIS 6-biome land cover map (grasses and cereal crops, shrubs, broadleaf crops, savannas, broadleaf forests and needleleaf forests) generated from one year of MODIS data [*Friedl et al.*, 2002]. The main MODIS operational LAI/FPAR algorithm accomplishes the inverse problem of retrieving LAI and FPAR on the basis of atmospherically corrected surface reflectance values and biome type. Failure of this main algorithm is circumvented by using a backup algorithm based on the relationships between NDVI and LAI/FPAR [*Knyazikhin et al.*, 1998]. The MODIS LAI and FPAR products are disseminated with their respective uncertainties given inputs of sun and view directions, biome type and observed red and near-infrared surface reflectance values with associated errors.

[14] Collection 4 of MODIS LAI from January 2001 through December 2004 was reprojected from the sinusoidal to a geographic projection, and was gridded at a 1° resolution and a monthly time step. Since the MODIS period does not overlap to the GSWP-2 period, we solely used these data for a qualitative assessment of the mean behavior of the model.

3. Model and Simulation

3.1. ISBA-A-gs Model

[15] The ISBA model (Interactions between Soil, Biosphere and Atmosphere [*Noilhan and Planton*, 1989; *Noilhan and Mahfouf*, 1996]) is a land surface model designed for use in numerical weather prediction models and climate models. The canopy is represented by a single vegetation layer (big-leaf model).

[16] A CO_2-responsive version of ISBA, called ISBA-A-gs [*Calvet et al.*, 1998], permits to account for the effect of the atmospheric carbon dioxide concentration and the interactions between all environmental factors on the stomatal aperture. ISBA-A-gs simulates g_s by considering the functional relationship between stomatal aperture and photosynthesis, on the basis of the biochemical A-gs model proposed by *Jacobs et al.* [1996] under well watered conditions (see Appendix A). The A-gs parameterization replaces the Jarvis-type [*Jarvis*, 1976] formulation of stomatal conductance of the standard version of ISBA. The model also includes a representation of the soil moisture stress. Two different types of drought responses are distinguished for both herbaceous vegetation [*Calvet*, 2000] and forests [*Calvet et al.*, 2004], depending on the evolution of water use efficiency (W_{UE}) under moderate stress: W_{UE} increases in the early stages of soil water stress in the case of the drought-avoiding response (also called "defensive" strategy), whereas W_{UE} decreases or remains stable in the case of the drought-tolerant response ("offensive" strategy).

[17] The ISBA-A-gs model can also simulate the green LAI by using a simple growth model [*Calvet and Soussana*, 2001] (see Appendix B). The model simulates only two aboveground biomass reservoirs: the leaf biomass B and the aboveground structural biomass B_s. The reservoirs are fed by the net assimilated carbon, and decreased by a turnover and a respiration terms. Phenology is modeled implicitly: LAI follows the variations of the leaf biomass, divided by the constant ratio α_B. The original formulation of α_B was not appropriate for the global scale, since the system needed to be iterated (for further details, see *Calvet and Soussana* [2001]). Moreover, for the global implementation the plas-

Table 1. Vegetation Parameters of ISBA-A-gs With the Nitrogen Option

Parameter Name	Symbol	Units
Unstressed mesophyll conductance at 25°C	g_m^*	mm s^{-1}
Potential leaf life expectancy	τ_M	day
Minimum leaf area index	$LAI_{\min}$	m^2 m^{-2}
Soil moisture stress response strategy		
Maximum leaf-to-air saturation deficit	$D_{\max}^*$	g kg^{-1}
Maximum value of the leaf [CO_2] ratio	f_0^*	
Cuticular conductance	g_c	mm s^{-1}
Critical extractable soil moisture	θ_C	
Nitrogen plasticity parameter (slope)	e	m^2 $kg^{-1}\%^{-1}$
Nitrogen plasticity parameter (intercept)	f	m^2 kg^{-1}
Leaf nitrogen concentration	N_l	%

ticity parameters e and f have to be estimated at the biome level, and must be determined by using the available information, i.e., estimates of Specific Leaf Area (SLA, the ratio between LAI and leaf biomass) and of leaf nitrogen concentration N_l (see section 3.2). Therefore α_B was redefined as being the ratio of the biomass of green leaves to LAI, i.e., the inverse of SLA:

$$\alpha_B = \frac{B}{LAI} = \frac{1}{SLA} = \frac{1}{eN_l + f}, \tag{1}$$

where e (in m^2 $kg^{-1}\%^{-1}$) and f (in m^2 kg^{-1}) are plasticity parameters, and N_l (in %) is the nitrogen concentration of the leaf biomass B.

3.2. Determination of the Model Parameters at a Global Scale

[18] The use of the nitrogen option of ISBA-A-gs at the global scale requires specifying 11 vegetation parameters (see symbols and units in Table 1). They must be determined for each vegetation type of the ECOCLIMAP database.

[19] The values of these parameters are summarized in Table 2. The asterisk symbol means that the value is derived for well watered, non-moisture-limiting conditions; the parameter value is modified by soil moisture stress. The mesophyll conductance g_m^* is a key parameter as it controls the photosynthesis in the model. A meta-analysis was performed by gathering optimized values for a great number of species from field observations [*Calvet*, 2000; *Calvet et al.*, 2004]. The values were grouped by vegetation types, and the statistics are presented in Table 3. The optimized values were obtained by minimizing the root mean square difference between simulated and measured g_s, i.e., by optimizing the water fluxes simulated by the model [*Calvet*, 2000; *Calvet et al.*, 2004]. Mean values from the meta-analysis were rounded and allocated to each vegetation type. The net assimilation rate produced with the mean value of g_m^* obtained for C_4 plants (6 mm s^{-1}) is not saturated under current atmospheric CO_2 concentration. *Poorter* [1993] reviewed the growth response of plants to an elevated CO_2 concentration, and showed that the growth of C_4 crops is not stimulated, unlike that of C_4 weed species. So g_m^* was increased to 9 mm s^{-1} for C_4 crops. Also, g_m^* was decreased to 2 mm s^{-1} for needleleaf trees and evergreen broadleaf trees to reflect the lower values compared to deciduous broadleaf trees found in the data [*Calvet et al.*, 2004]. The resulting values of g_m^* in Table 2 are still close to the mean value of the corresponding class (Table 3) for most of the vegetation types, and always between the lower and the upper quintile. The potential leaf life expectancy τ_M controls the turnover rates of the leaf and the structural biomass pools. The values of τ_M in Table 2 were fixed from values used in previous studies [*Rivalland et al.*, 2005; *Voirin et al.*, 2001; *Calvet et al.*, 1998]. They are comparable with leaf span time data published by *Reich et al.* [1999]. A minimum LAI value, $LAI_{\min}$, is needed to calculate a minimum level of photosynthesis at the start of the growing season. $LAI_{\min}$ was arbitrary fixed at 1 m^2 m^{-2} for evergreen broadleaf trees and needleleaf trees, and at 0.3 m^2 m^{-2} for the other vegetation types. $LAI_{\min}$ is sufficiently low to simulate a possible interannual variability of the minimum values of LAI simulated by the model, depending on climatic conditions. For herbaceous species, the maximum leaf-to-air saturation deficit $D_{\max}^*$ was calculated from the value of g_m^*, and the maximum ratio between the intercellular and the atmospheric CO_2 concentration f_o^* was set to a constant value [*Calvet*, 2000] (see Appendix C). For woody species, f_o^* was variable and derived from g_m^* [*Calvet*, 2000] (see Appendix C). As far as $D_{\max}^*$ is concerned, a new regression relationship with g_m^* was established from the data published by *Calvet et al.* [2004] for woody species:

$$D_{\max}^* = -37.97 \ln(g_m^*) + 150.4, \tag{2}$$

with g_m^* in mm s^{-1} and $D_{\max}^*$ in g kg^{-1}. This relationship results in lower sensitivity of stomatal aperture to air humidity at low values of g_m^*.

Table 2. Values of ISBA-A-gs Parameters for the ECOCLIMAP Vegetation Types[a]

Vegetation Type	g_m^*	τ_M	$LAI_{\min}$	$D_{\max}^*$	f_0^*	g_c	θ_C	e	f	N_l
Deciduous broadleaf trees	3	230	0.3	109	0.51	0.15	0.3	4.83	2.53	2
Evergreen broadleaf trees	2	365	1	124	0.57	0.15	0.3	4.83	2.53	2.5
Needleleaf trees	2	365	1	124	0.57	0	0.3	4.85	−0.24	2.8
C_3 crops	1	150	0.3	50	0.95	0.25	0.3	3.79	9.84	1.3
C_4 crops	9	150	0.3	33	0.6	0.15	0.3	7.68	−4.33	1.9
Irrigated crops	9	150	0.3	33	0.6	0.15	0.3	7.68	−4.33	1.9
C_3 natural herbaceous	1	150	0.3	50	0.95	0.25	0.3	5.56	6.73	1.3
C_4 natural herbaceous	6	150	0.3	52	0.6	0.15	0.3	7.68	−4.33	1.3
Irrigated herbaceous	1	150	0.3	50	0.95	0.25	0.3	5.56	6.73	1.3

[a] g_m^* is in mm s^{-1}, τ_M is in days, $LAI_{\min}$ is in m^2 m^{-2}, is $D_{\max}^*$ is in g kg^{-1}, f_0^* is dimensionless, g_c is in mm s^{-1}, θ_C is dimensionless, e is in m^2 $kg^{-1\%-1}$, f is in m^2 kg^{-1}, and N_l is in %.

Table 3. Statistics on Optimized Values of g^*_m for Herbaceous Vegetation [*Calvet*, 2000] and Woody Vegetation [*Calvet et al.*, 2004][a]

Vegetation Class	m	Q_{20}	Q_{80}
Woody vegetation	3.5	0.2	5.1
C_3 herbaceous vegetation (natural and crops)	0.8	0.3	1.1
C_4 herbaceous vegetation (natural and crops)	6.4	1.3	12.6

[a]Unit is mm s^{-1}; m, mean; Q_{20}, lower quintile; and Q_{80}, upper quintile.

[20] The values of cuticular conductance g_c were taken from *Calvet* [2000] and *Calvet et al.* [2004]. The soil moisture stress response is species-dependent: soybean and cowpea were found drought-avoiding while sunflower and a temperate grassland were found drought-tolerant by *Calvet* [2000]; for tree species, maritime pine appeared to be drought-avoiding, as sessile oak revealed itself drought-tolerant in the work by *Calvet et al.* [2004]. Therefore it was difficult to prescribe a single response for a whole ecosystem, and two global simulations were performed using drought-avoiding and drought-tolerant strategies respectively. Because the differences in calculated LAI between the two simulations were small, only the drought-avoiding simulation is compared against the satellite data sets in this study. The nitrogen plasticity parameters e and f were estimated as the coefficients of the linear regression relationship (equation (1)) between SLA and N_l values compiled by *Schulze et al.* [1994], *Reich et al.* [1999] and *Rivalland* [2003]. The foliar nitrogen concentration N_l was tuned during preliminary simulations to get realistic values of annual GPP (gross primary production) for a broad range of climate conditions for each of the vegetation types. GPP was estimated as twice the NPP (net primary production) given by *Prentice et al.* [2001]. NPP could not be compared directly, as ISBA-A-gs does not simulate underground biomass and respiration. For certain types of vegetation, the tuned values of N_l (Table 2) are different from the typical nitrogen content measured in the field [*Schulze et al.*, 1994; *Reich et al.*, 1999; *Rivalland*, 2003; *Reich and Oleksyn*, 2004]. Actually, it is more relevant to compare SLA values, as it is the variable used in the model to calculate LAI from the leaf biomass. The measured values of SLA [*Schulze et al.*, 1994; *Reich et al.*, 1999; *Rivalland*, 2003] were grouped by vegetation types, and compared with the model values of SLA (calculated from e, f and N_l according to equation (1)) in Table 4. SLA values in the model are lower than observations for C_3 herbaceous and C_3 crops, and higher for needleleaf and evergreen broadleaf trees. Nevertheless, the resulting SLA values are in the observed range of the pool of data, and the difference between the model values and the mean observed values is generally lower than the standard deviation of the observations.

[21] This set of parameters allows to differentiate the response of the 9 vegetation types in ECOCLIMAP (namely, herbaceous and woody types, or C_3 and C_4 photosynthesis pathway). ISBA-A-gs also permits to simulate the influence of the various climate conditions on the vegetation growth.

3.3. Design of the Global Simulation

[22] The ISBA-A-gs model was run at a global scale, with a 1° horizontal resolution, forced by the GSWP-2 meteorological data from July 1982 to December 1995. As the correction of precipitation values changed in January 1986 (see section 2.1), the years before this date are used as a spin up period, and the simulation is analyzed for the 1986–1995 period, only. The atmospheric CO_2 concentration was set to 350 ppm.

[23] The model was run in its tile version: in each grid box, the model simulates the evolution of the prognostic variables for each vegetation type that is present in the grid box. In the following, the LAI values shown for the model simulation and the ECOCLIMAP data set are averaged grid box values, calculated as the means of the tile values weighted by their relative fraction, including bare soil. These averages are comparable to the values of the other satellite data sets.

[24] Soil and vegetation parameters were initialized with the ECOCLIMAP data fields, including parameters determined in section 3.2.

4. Validation of Simulated LAI at a Global Scale

[25] In this section, the simulated LAI is compared against three global data sets derived from satellite data: ISLSCP-II, MODIS and ECOCLIMAP. The main advantage of the ISLSCP-II data set is that it is available during the whole simulation period, representing a large interannual variability. MODIS is a new generation product, but only four full years (2001–2004) outside the simulation period were available. Average MODIS values are used here as a climatology to validate the mean LAI. The ECOCLIMAP monthly climatology of LAI is used in the same manner.

[26] There are several limitations in the satellite observations and in the model that can explain discrepancies between the various LAI data sets:

[27] 1. The remote sensing LAI products are estimates derived from top-of-the-atmosphere reflectances, and use different sensors and algorithms [*Los et al.*, 2000; *Myneni et al.*, 2002]. The quality of LAI retrievals is limited by the intrinsic characteristics of the sensor systems, the dynamic of the signal received at the satellite level, and the physical properties of the target. For instance, the visible signal saturates for high levels of light absorption, which makes it difficult to estimate accurate LAI values beyond 3 or 4. Cloud cover hides the surface and produces discontinuities in time series. Moreover, the LAI measurement from space may be affected by the scanning and illumination geome-

Table 4. SLA Values Used in the Model (SLA_M), Mean Values (SLA_O) and Standard Deviations (SD_O) Calculated From the Pool of Data Published by *Schulze et al.* [1994], *Reich et al.* [1999] and *Rivalland* [2003][a]

Vegetation Type	SLA_M	SLA_O	SD_O
Deciduous broadleaf trees	12.2	14.1	6.6
Evergreen broadleaf trees	14.6	8.3	3.5
Needleleaf trees	13.3	7.0	4.0
C_3 crops	14.8	22.5	7.6
C_4 crops	10.3	9.9	7.9
C_3 natural herbaceous	14.0	20.2	11.0
C_4 natural herbaceous	5.7	9.9	7.9

[a]Unit is m^2 kg^{-1}.

tries. Indeed, the layers of a vegetation canopy cast shadow and LAI of lower layers near the ground may not be well documented. This may yield underestimate by 30% in the case of clumped canopies [*Roujean and Lacaze*, 2002]. This occurs mostly for dense forested areas and fully developed crops. On the other hand, over semiarid ecosystems, soil brightness contaminates sufficiently the signal to restrict its sensitive response to LAI increase. Similarly, high reflectance of snow may hamper an accurate LAI retrieval at high latitudes at springtime.

[28] 2. The satellite-derived LAI is scaled according to in situ measurements. Here again, the LAI definition, the methods and instruments used, the sampling, and the canopy structure are some of the sources of uncertainty [*Asner et al.*, 2003; *Jonckheere et al.*, 2004].

[29] 3. Satellite-derived LAI represents total (living and senescent) single-sided leaf area surface per column unit, when simulated LAI corresponds to photosynthetically active leaves (in fact, green LAI is also provided in ISLSCP-II and ECOCLIMAP data sets and is used for the comparison, but green LAI is not available in MODIS).

[30] 4. The quality of the atmospheric forcing is not spatially homogeneous and depends on the observation network density. In particular, existing global fields of precipitation estimates are highly scattered, and precipitation controls photosynthesis over large regions of the Earth.

[31] 5. The modeling approach we used in this study has also some limitations: parameterizations are simplified representation of the processes of the real world (for example, the complex biochemical reactions involved in photosynthesis are described by a set of a few empirical equations); some processes are not represented (for example, the undergrowth in forests is not simulated by a one-big-leaf model).

[32] 6. Moreover, the choice of the same parameter for one whole type of vegetation is a simplification, and does not allow taking into account the interspecific variability, or the plant adaptation to environmental factors.

[33] However, comparing the simulated LAI with satellite data is the only way to validate the model at the global scale.

4.1. Mean Maximum of LAI

[34] The mean behavior of the model is analyzed by comparing the simulated maximum of LAI with the satellite-derived data sets. Maximum of LAI was chosen as it generally occurs simultaneously with the maximum evapotranspiration rate, and reflects the yearly accumulation of carbon by the vegetation.

[35] Figure 1 shows the mean of the yearly maximum LAI of the model and of the three satellite data sets (mean of the maximum monthly values over the available years of the data sets on a per-pixel basis). The model captures the main features of the global pattern. Biomes characterized by high LAI values (tropical and boreal forests, croplands) appear clearly. This is to some extent the consequence of using the land use prescribed from ECOCLIMAP (besides, differences in LAI values can occur for a few grid cells at the boundary of two biomes, because of the possible inconsistency of land use in the data sets). However, this also shows the ability of ISBA-A-gs to respond to various climate conditions: the model represents the precipitation-driven east-western gradient over North America and the north-southern gradient over central Africa, as well as the temperature-driven gradients over mountainous regions, for example around the Andes or the Himalayas. The comparison of the satellite data sets with one another raises the difficulty to validate LAI at the global scale as differences can reach more than 2 m^2 m^{-2} in latitudinal means between ISLSCP-II and MODIS (Figure 2). The simulated LAI is generally between the various satellite estimates (Figure 2). Large differences between the model and ISLSCP-II are found over coniferous boreal forests (Figure 1 and Table 5), as in the works by *Kergoat et al.* [2002] and *Dickinson et al.* [1998]. This can reveal a model bias for this biome (the tuned value of N_l is out of the range of the observed values for this biome, see section 3.2). However, LAI values of 8 m^2 m^{-2} are very high even for in situ observations, and may not be representative of a model grid cell of $1° \times 1°$. Moreover, values of maximum of LAI are lower in both the ECOCLIMAP and MODIS data sets (Table 5). To a lesser extent, similar results are found for the other woody vegetation types (tropical evergreen broadleaf forests and temperate deciduous broadleaf forests) in Figure 1 and Table 5. A better agreement is found for herbaceous vegetation types. For C_4 grasslands in tropical regions, the model overestimates LAI values in comparison with all the satellite data sets (for example over sub-Saharan Africa, see Table 5). This can be due to the fact that the model uses the same optimum photosynthesis temperature for each vegetation type all around the world (32°C). In the tropics, temperature is close to the model optimum for long periods of time and therefore favors high rates of carbon assimilation. Other models [e.g., *Krinner et al.*, 2005] take into account the adaptation of the plants to their environment by varying the optimum temperature according to climate conditions. At the global scale, the differences between the modeled LAI and the observed data sets are less than those obtained by *Dan et al.* [2005] in a coupled atmosphere-biosphere simulation. Table 5 also confirms that the model is able to represent the spatial variability found in the observations: the model spatial standard deviations are comparable to the observations ones. Weaker spatial variability in ECOCLIMAP is inherent to the method of assigning the same LAI characteristics to a whole ecosystem [*Masson et al.*, 2003].

4.2. Interannual LAI Variability

[36] Many studies have addressed the link between variations in the climate and in the vegetation activity inferred from remote sensing measurements [e.g., *Myneni et al.*, 1997; *Zhou et al.*, 2001, 2003; *Buermann et al.*, 2002; *Gong and Shi*, 2003; *Nemani et al.*, 2003]. In ISBA-A-gs, the simulated LAI responds to the temporal variability of the climate. In this section, the ISLSCP-II data set, spanning the simulation period, is used to validate the model's interannual variability.

[37] Correlation between the model and the observations of the monthly deseasonalized LAI anomalies is shown on Figure 3 (monthly time series of the anomaly from the mean annual cycle). The modeled LAI correlates well with the observations, with a significant positive Pearson's correlation (at a 90% level) for 64% of the grid points, forming regional coherent patterns. The correlation is high over

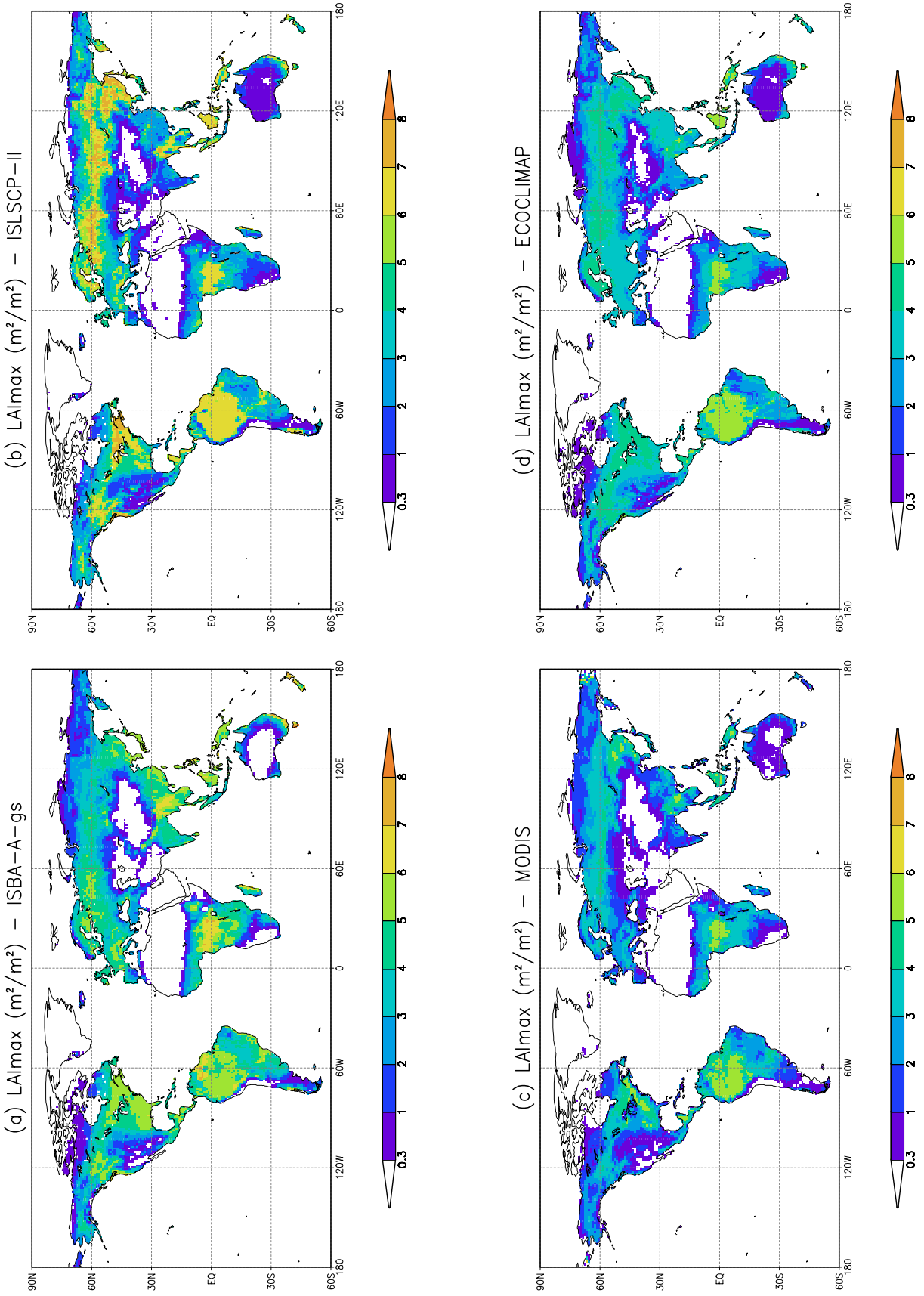

Figure 1. Maximum of LAI (a) simulated by ISBA-A-gs (mean 1986–1995) and derived from the (b) ISLSCP-II data set (mean 1986–1995), (c) MODIS data set (mean 2001–2004), and (d) ECOCLIMAP data set (climatology).

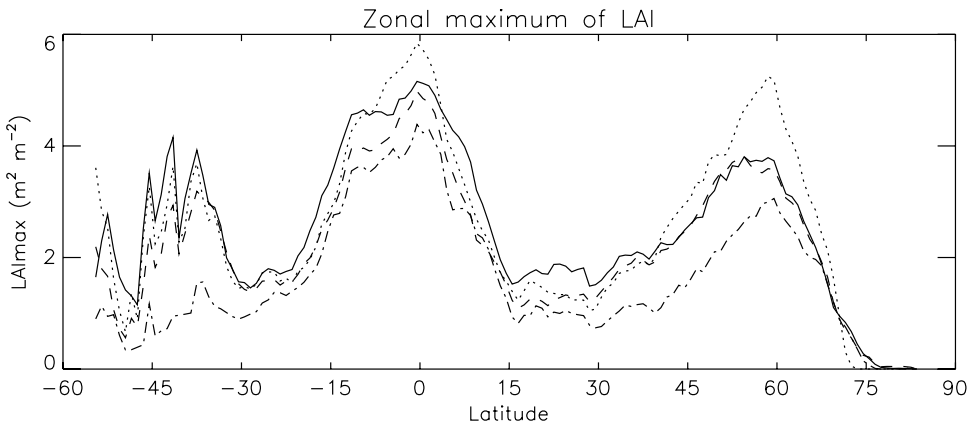

Figure 2. Zonal mean of the maximum of LAI: simulated by ISBA-A-gs (mean 1986–1995) (solid), ISLSCP-II data set (mean 1986–1995) (dotted), MODIS data set (mean 2001–2004) (dash-dotted), ECOCLIMAP data set (climatology) (dashed).

semiarid areas (e.g., Australia, south of Africa, west of North America, Sahel, and Mediterranean basin), showing that the model simulates well the response of photosynthesis to the air and soil water stresses, and also the soil water dynamics over these areas. For example, over south of Africa (covered mainly by C_4 grasslands), the model reproduces well both monthly LAI and LAI anomaly, thanks to the high correlation with rainfall rate (Figure 4), as found by *Richard and Poccard* [1998]. The precipitation over this region is correlated with El Niño–Southern Oscillation (ENSO): the climate is dryer during El Niño events, in 1986–1987 and in 1991–1992, and wetter during La Niña, in 1988. This skill of the model in the Sahel is particularly promising as *Zeng et al.* [1999] showed that taking into account vegetation interaction permits to enhance the simulation of rainfall interdecadal variability by a climate model over this region.

[38] The correlation is lower over tropical broadleaf evergreen forests in Africa and in Indonesia, because of a much larger annual amplitude in ISLSCP-II than in the model (Figure 5). Intra-annual variability is low in the simulation because of favorable environmental conditions for photosynthesis all along the year in the tropics. This is not an evidence of a model failure, as the quality of the satellite products is questionable in the tropics because of the frequent cloud cover of the Intertropical Convergence Zone (ITCZ) and the saturation in NDVI. Moreover, the annual amplitude in the model is comparable to the other satellite data sets (not shown).

[39] The correlation between ISBA-A-gs and the ISLSCP-II LAI is low over northern and central Europe, despite the high correlation with the air temperature during the growing season found in both the model and the observations (not shown). Over central Europe (covered mainly by C_3 crops, broadleaf deciduous forests and needleleaf forests), this low correlation is produced by opposite anomalies occurring for a few years where the LAI anomaly in the model is driven by soil moisture (Figure 6). Main differences in LAI anomaly occur in 1987, 1988, 1992 and 1994, and can be explained by variations in the soil wetness index (normalized soil moisture content in the root-zone, ranging from 0 at wilting point to 1 at field capacity). In 1992 and 1994, the negative anomaly in soil water content could have been compensated by irrigation over croplands, but this process is not simulated by the model. Over Scandinavia (covered by needleleaf forests and C_3 grasslands), the low correlation is due to a high variability in maximum of LAI in ISLSCP-II that is not reproduced by the model, reflecting a low variability in the atmospheric forcing (not shown).

4.3. Start of the Growing Season

[40] Predicting the vegetation phenology is also a challenge. In particular, the start of the growing season triggers an increase in the latent heat flux part in the energy budget,

Table 5. Statistics on Maximum of LAI for the Model and the Satellite Data Sets: Spatial Average, (Spatial Standard Deviation), for Several Regions and Associated Vegetation Types[a]

Vegetation Type	Location	*n*	ISBA	ISLSCP2	ECOCLIMAP	MODIS
Deciduous broadleaf trees	western USA [30°N:50°N;−100°E:−60°E]	78	5.2 (0.5)	6.8 (0.6)	4.2 (0.3)	4.6 (1)
Evergreen broadleaf trees	Amazonia [−20°N:20°N;−80°E:−30°E]	564	5.4 (0.6)	6.6 (0.7)	5.5 (0.6)	4.8 (0.8)
Needleleaf trees	northern Europe and Russia [50°N:70°N;0°E:90°E]	406	4.6 (0.7)	6 (1.4)	4.3 (0.6)	3.4 (0.9)
C_3 crops	Europe [40°N:60°N;0°E:60°E]	365	3.7 (0.8)	3.4 (0.7)	3.7 (0.2)	1.9 (0.7)
C_4 crops	western USA [40°N:50°N;−110°E:−80°E]	55	4 (0.9)	4.2 (0.7)	3.9 (0.2)	2.1 (0.4)
C_3 natural herbaceous	high latitudes [50°N:75°N;−180°E:180°E]	2168	2.3 (1.4)	2.8 (2)	2.1 (1.2)	1.9 (1.2)
C_4 natural herbaceous	sub-Saharan Africa [5°N:20°N;−20°E:50°E]	379	2.6 (1.3)	2.2 (1)	2.2 (0.8)	2.2 (0.9)

[a]Unit is $m^2\ m^{-2}$; *n* is the number of grid points selected in the area, where the fraction of the vegetation type is higher than 0.5. LAI values are weighted by the surface of the grid cell.

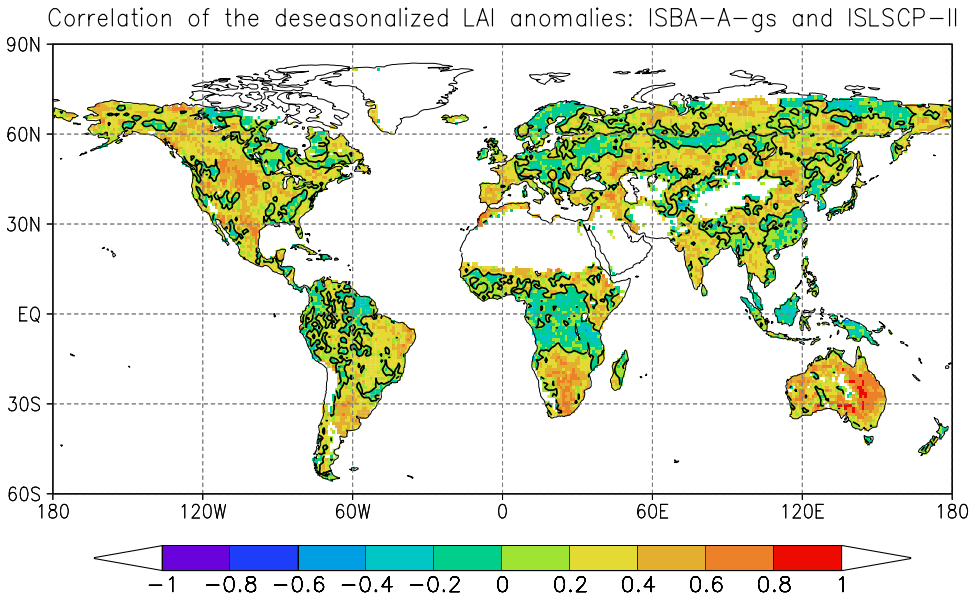

Figure 3. Correlation of the monthly deseasonalized LAI anomalies between ISBA-A-gs and the ISLSCP-II data (1986–1995). The threshold value of significant positive correlation at 90% is contoured.

and the beginning of the net absorption of carbon by vegetation. For example, *Bondeau et al.* [1999] showed the importance of the vegetation phenology to predict the seasonal variations of NPP. The 10-day time step of ISLSCP-II data was useful to determine the date of the start of the growing season. This date was computed as the decade when (LAI - minimum of LAI) became higher than 40% of the amplitude of the annual cycle. A similar algorithm has been used by *White et al.* [1997]. The relatively high threshold avoided the confusion with the start of the satellite NDVI due to snowmelt at high latitudes [*Moulin et al.*, 1997]. The grid points where the annual LAI amplitude is less than 0.5 m^2 m^{-2} were ignored, as well as those where the start decade occurred alternatively at the end or at the beginning of the year. The same algorithm was applied to the simulated LAI, using the mean grid cell value (Figure 7). Again, the model is able to capture the main features of the spatial pattern of ISLSCP-II data set: the latitudinal gradient over northern Asia and Europe, tropical Africa, or east of northern America, and also the late values over India and southeastern Asia. However, the detected onset dates generally occur later in the model than in the observations, except in southeastern Asia and east of northern America (Table 6). The delay is up to four decades over western Europe and west of tropical Africa. The flaws described in section 4 can explain such a shift. For example, *Wang et al.* [2005] found an advance of 11 to 40 days in the onset of vegetation in MODIS data in comparison with in situ measurements at two European deciduous broadleaf forests sites, and imputed it to the undergrowth. Also, the model does not simulate grazing in grasslands, nor agricultural practices (namely, sowing and harvesting dates or irrigation), which have a direct influence on the growing cycle of the cultural areas over central and western Europe, east of northern America, India and southeastern Asia. At high latitudes, the model simulates a late snowmelt, which maintains too low surface temperatures at spring, preventing photosynthesis to occur. B. Decharme and H. Douville (Global validation of the ISBA sub-grid hydrology, submitted to *Climate Dynamics*, 2006) showed that the simulation of the date of snowmelt, and consequently the river discharge, was improved by using a more complex snow scheme in ISBA. Over sub-Saharan Africa, the vegetation cannot grow on time because of a severe soil moisture limitation, suggesting problems in the precipitation forcing or in the representation of the soil hydrology by the model. Vegetation rapidly reacts to precipitation in these areas, but in the model, an amount of water is first used to refill the soil water content depending on the rooting depth. The value of 1.5 m in ECOCLIMAP may be overestimated for these regions.

[41] Differences of one or a few decades can seem huge when compared to the few days performed at isolated sites by recent phenology parameterizations [e.g., *Arora and Boer*, 2005; *Jolly et al.*, 2005]. However, ISBA-A-gs does not simulate phenology explicitly: leaves' growth simply follows the balance between assimilation and losses of carbon. Moreover, phenology is validated at a global scale in this study, and the model results are comparable to those obtained by *Botta et al.* [2000] using a prognostic scheme depending on the vegetation type. Finally, the model also captures the interannual variability in the start of the growing season. It simulates a temporal amplitude comparable to ISLSCP-II in the date of leaf onset (Table 6). Over the globe, 46% of the grid points show a significant positive correlation between the model and the observations at the 90% level.

[42] *Myneni et al.* [1997] observed a lengthening of the growing season at mid and high latitudes of Northern Hemisphere from 1981 to 1991. *Zhou et al.* [2001] and *Zhou et al.* [2003] found similar variations in the northern vegetation activity from 1982 to 1999. Also, *Nemani et al.* [2003] found an increase in terrestrial net primary production for the same period. These changes were attributed to

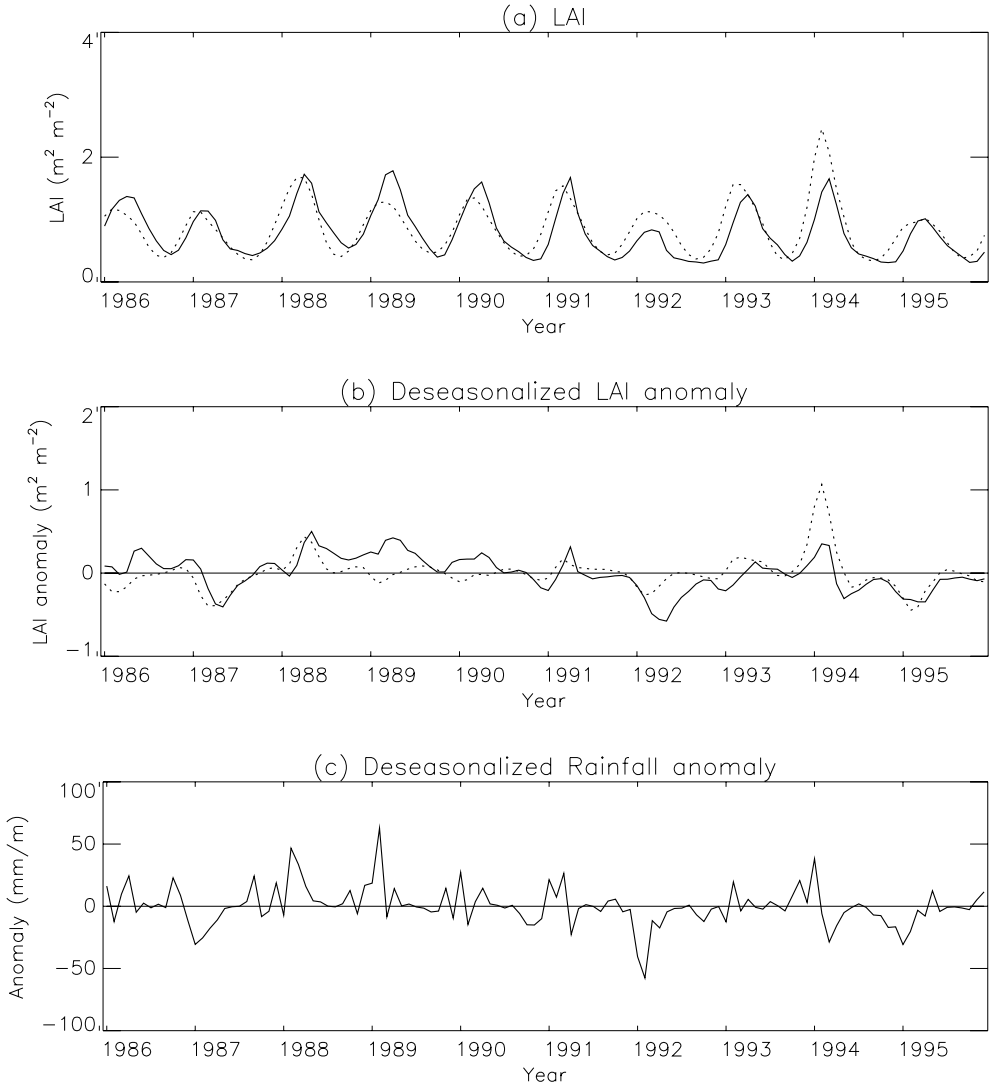

Figure 4. Monthly time series of (a) LAI for ISBA-A-gs (solid) and ISLSCP-II (dotted), (b) deseasonalized LAI anomaly (idem), and (c) deseasonalized GSWP-2 rainfall anomaly (solid) over south of Africa [−35°N:−15°N, 10°E:40°E].

temperature changes [*Zhou et al.*, 2001, 2003]. Indeed, the increase in atmospheric CO_2 concentration is not sufficient to explain such changes in biological activity. We investigated the variability of the date of beginning of the growing season over this area for the 1986–1995 period, but we were not able to find any clear trend neither in the model nor in the observations (Figure 8). In fact, it seems that 1986–1995 is a transition period with no detectable trend in

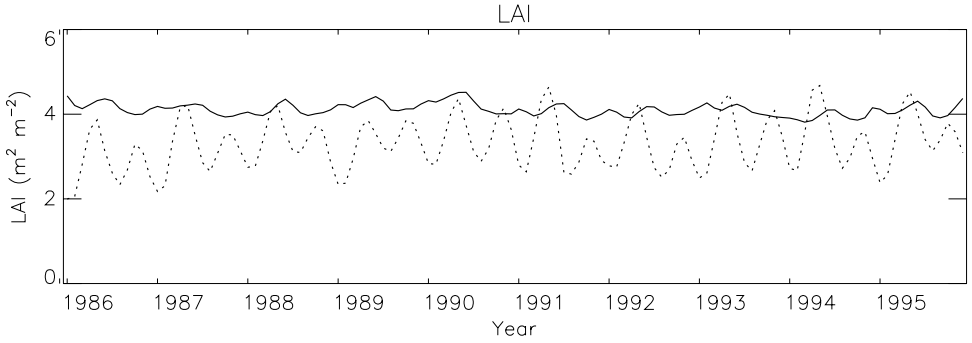

Figure 5. Monthly time series of LAI for ISBA-A-gs (solid) and ISLSCP-II (dotted) over tropical Africa and Indonesia [−5°N:5°N, 0°E:180°E].

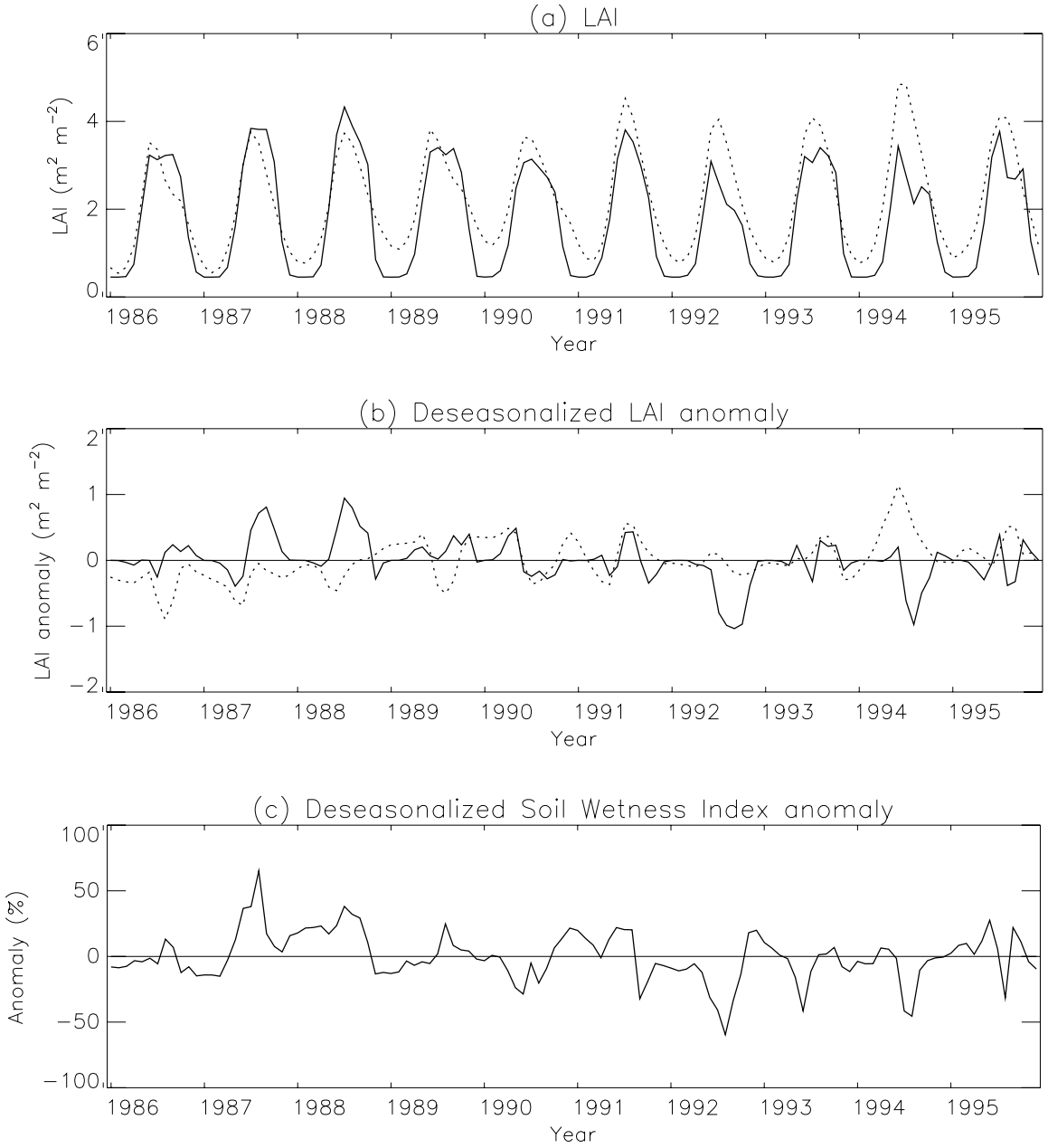

Figure 6. Monthly time series of (a) LAI for ISBA-A-gs (solid) and ISLSCP-II (dotted), (b) deseasonalized LAI anomaly (idem), and (c) deseasonalized soil wetness index anomaly (solid) over central Europe [45°N:60°N, 10°E:30°E].

NDVI or temperature, because of a cooling in 1992 after the 1991 eruption of Mount Pinatubo. It can be noted that vegetation systematically starts later in the model because of the delayed snowmelt (see last section), but the annual variations are in good agreement.

5. Conclusion

[43] In the present study, a 10-year forced simulation was performed at a global scale for the 1986–1995 period to simulate the response of vegetation to climate, by using the land surface model ISBA-A-gs, and the ECOCLIMAP surface parameters database. The simulated LAI is favorably compared with three satellite-derived LAI data sets (ISLSCP-II, MODIS and ECOCLIMAP). The results also compare satisfactorily to LAI simulated by global models in other studies.

[44] The model is able to capture the main spatial patterns of LAI, in agreement with the satellite estimates, though significant differences are found between the various satellite data sets. The highest and lowest LAI values are generally obtained for ISLSCP-II and MODIS, respectively. Such discrepancies can be due to differences in sensor characteristics, in retrieval methods of LAI and in the considered periods of the selected data sets. Although the model provides a simplified representation of the vegetation dynamics, the deviations between simulated and satellite-derived LAI are less than the discrepancies between the

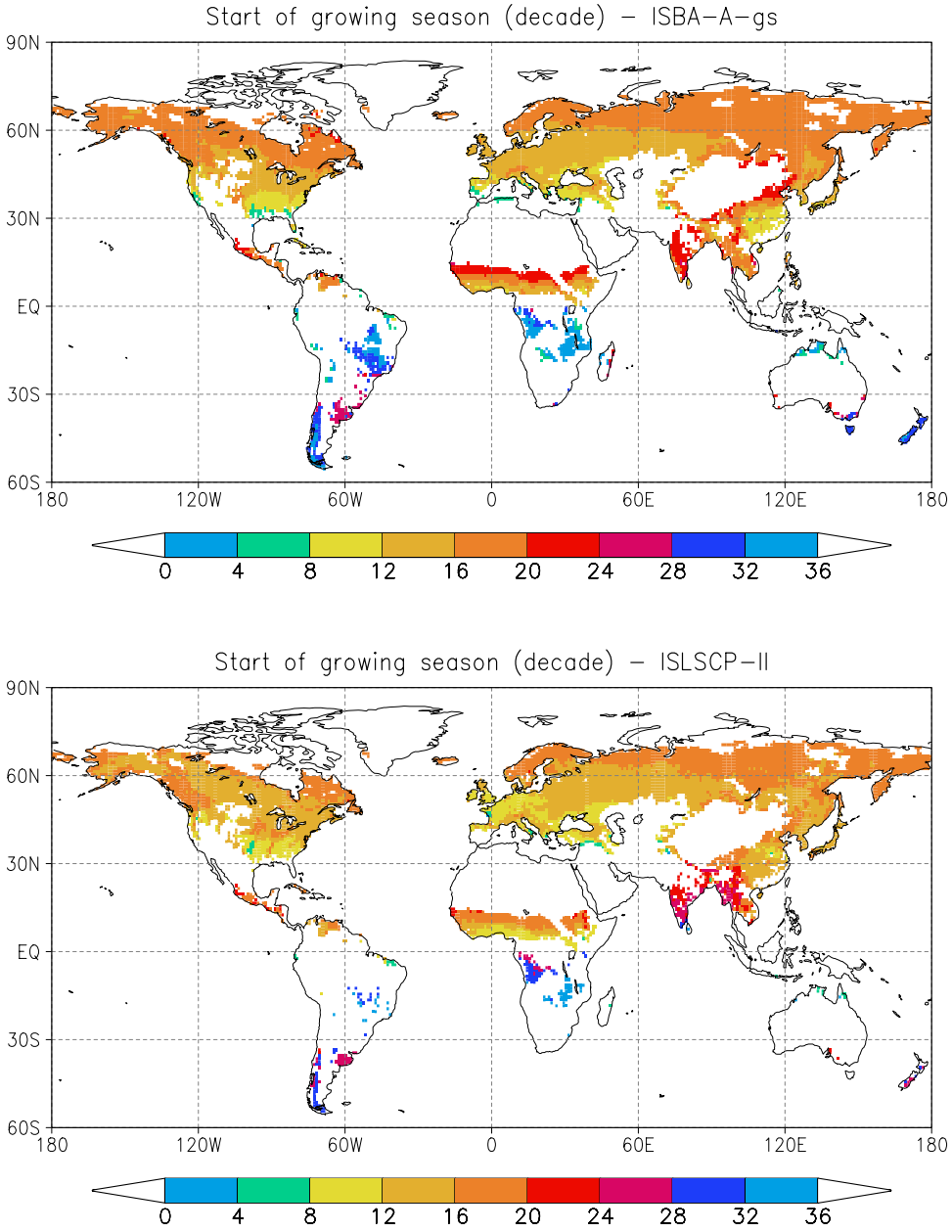

Figure 7. Date of start of the growing season (mean 1986–1995) (top) simulated by ISBA-A-gs and (bottom) observed in ISLSCP-II.

various LAI estimates. The model also responds to the temporal and spatial variations in atmospheric forcing. The interannual variability is reproduced well over several regions of the globe, particularly in those where precipitation controls photosynthesis. Over tropical and boreal forests, the variability in ISLSCP-II seems overestimated compared to the climate variability, and is not reproduced by the model. As the model does not simulate processes

Table 6. Statistics on the Date of Leaf Onset for the Model and the ISLSCP-II Data Set: Spatial Average, (Spatial Average of 1986–1995 Minimum/Maximum), for Several Regions and Associated Vegetation Types[a]

Vegetation Type	Location	*n*	ISBA	ISLSCP2
Deciduous broadleaf trees	western USA [30°N:50°N;−100°E:−60°E]	78	140 (131/149)	127 (112/140)
Needleleaf trees	northern Europe and Russia [50°N:70°N;0°E:90°E]	406	164 (153/174)	159 (138/177)
C_3 crops	Europe [40°N:60°N;0°E:60°E]	363	132 (116/145)	123 (103/141)
C_4 crops	western USA [40°N:50°N;−110°E:−80°E]	48	139 (120/165)	163 (148/176)
C_3 natural herbaceous	high latitudes [50°N:75°N;−180°E:180°E]	1446	177 (166/188)	163 (151/175)
C_4 natural herbaceous	sub-Saharan Africa [5°N:20°N;−20°E:50°E]	379	191 (170/213)	163 (141/186)

[a]Unit is days; *n* is the number of grid points selected in the area, where the fraction of the vegetation type is higher than 0.5 (the algorithm did not detect enough grid points for the evergreen broadleaf trees). Date values are weighted by the surface of the grid cell.

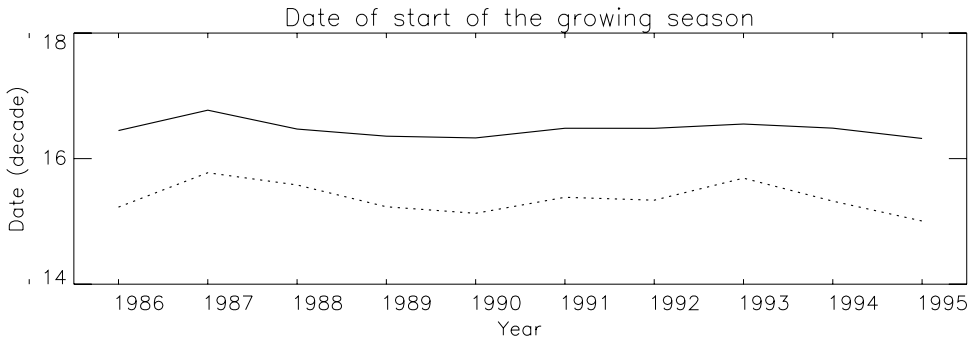

Figure 8. Annual time series of the date of start of the growing season for ISBA-A-gs (solid) and ISLSCP-II (dotted) over middle and high latitudes of the Northern Hemisphere [45°N:70°N, −180°E:180°E].

such as harvest or irrigation, the modeled variability is driven by the climate forcing, only, and may differ from the observed one in cultivated areas. Despite no explicit representation of phenology is used, the latitudinal pattern of the growing season onset matches the observations, although the growing season often begins later in the model than in the observations.

[45] Differences between the various observed data sets raise the difficulty to validate LAI at the global scale. However, comparison with satellite products is the only way to assess the realism of spatial and temporal variations simulated by the model. In that respect, it is necessary to reduce the uncertainty in satellite LAI estimates. This study also highlights the importance of the quality of the atmospheric forcing and of the biogeophysical parameters used in the model, and suggests further model improvements, namely in the snow dynamics or the treatment of vegetation in cultivated areas. Finally, this study shows that the ISBA-A-gs model is able to simulate realistic LAI time series at a global scale. It is now foreseen to couple ISBA-A-gs with ARPEGE-Climat, the atmospheric general circulation model of Météo-France [*Déqué et al.*, 1994; *Gibelin and Déqué*, 2003], to investigate the two-way interactions between vegetation and climate. It is also planned to couple ISBA-A-gs with a soil respiration model, in order to simulate the whole terrestrial carbon cycle.

Appendix A: A-gs Model

[46] The A-g_s approach employed to describe the leaf-scale physiological processes in ISBA-A-g_s [*Calvet et al.*, 1998] was the model proposed by *Jacobs et al.* [1996], assuming a well watered soil.

[47] The photosynthesis rate in light-saturating conditions is expressed as

$$A_m = A_{m,\max}\left[1 - \exp\left\{-g_m^* \times (C_i - \Gamma)/A_{m,\max}\right\}\right]. \qquad \text{(A1)}$$

[48] The g_m^* parameter (the unstressed mesophyll conductance) is corrected for leaf temperature using a Q_{10}-type function, together with the maximum photosynthesis $A_{m,\max}$. and the compensation point Γ. Typical values of $A_{m,\max}$ and Γ at a temperature of 25°C, for C_3 and C_4 plants, are given in Table A1. To avoid lengthy iterations, the internal CO_2 concentration C_i is obtained by combining the air CO_2 concentration C_s and Γ through the following closure equation

$$C_i = f\,C_s + (1 - f)\Gamma, \qquad \text{(A2)}$$

where the coupling factor f is sensitive to air humidity and depends on the cuticular conductance g_c and on g_m^*, f_0^* and $D_{\max}^*$ by

$$f = f_0^*(1 - D_s/D_{\max}^*) + (g_c/[g_c + g_m^*])(D_s/D_{\max}^*), \qquad \text{(A3)}$$

where D_s is the leaf-to-air saturation deficit, and f_0^* is the value of f for $D_s = 0$ g kg^{-1} (Table 2).

[49] The net assimilation is limited by a light deficit according to a saturation equation applied to the photosynthetically active radiation I_a:

$$A_n = (A_m + R_d)[1 - \exp\{-\varepsilon I_a/(A_m + R_d)\}] - R_d, \qquad \text{(A4)}$$

where leaf respiration is given by $R_d = A_m/9$, and the light conversion efficiency by $\varepsilon = \varepsilon_0(C_i - \Gamma)/(C_i + 2\Gamma)$, where ε_0 is the maximum quantum use efficiency (Table A1).

Table A1. Standard Values of the Parameters of the A-g_s Model, According to the Plant Type (C_3 or C_4), Adapted From *Jacobs et al.* [1996][a]

Parameter (X)	X(@25)	Q_{10}	T_1, °C	T_2, °C
C_3				
ε_0, mg J^{-1}	0.017			
Γ, ppm	45	1.5		
g_m^*, mm s^{-1}	see Table 2	2.0	5	36
$A_{m,\max}$, mg m^{-2} s^{-1}	2.2	2.0	8	38
C_4				
ε_0, mg J^{-1}	0.014			
Γ, ppm	2.8	1.5		
g_m^*, mm s^{-1}	see Table 2	2.0	13	36
$A_{m,\max}$, mg m^{-2} s^{-1}	1.7	2.0	13	38

[a] ε_0 is the maximum quantum use efficiency, Γ the compensation point, g_m^* the mesophyll conductance, and $A_{m,\max}$ the maximum net assimilation of the leaf. The Q_{10}, T_1 and T_2 values modulate the sensitivity of each parameter to temperature through either $X(T_s) = X(@25) \times Q_{10}^{(Ts\,-\,25)/10}$ for Γ or $X(T_s) = X(@25) \times Q_{10}^{(Ts\,-\,25)/10}/\{[1 + \exp\{0.3(T_1 - T_s)\}]\,[1 + \exp\{0.3(T_s - T_2)\}]\}$ for g_m^* and $A_{m,\max}$, where $X(T_s)$ and $X(@25)$ are the values of the parameters corresponding to the leaf temperatures T_s and 25°C, respectively.

[50] Finally,

$$g_s = g_c + 1.6\left(A_n - A_{\min}\left(\frac{D_s}{D^*_{\max}}\frac{A_n + R_d}{A_m + R_d}\right) + R_d\left(1 - \frac{A_n + R_d}{A_m + R_d}\right)\right)\Big/(C_s - C_i), \quad \text{(A5)}$$

where $A_{\min}$ represents the residual photosynthesis rate (at full light intensity) associated with cuticular transfers when the stomata are closed because of a high saturation deficit:

$$A_{\min} = g^*_m \times g_c(C_s - \Gamma)/(g^*_m + g_c). \quad \text{(A6)}$$

[51] From the above equations, the water use efficiency (i.e., the ratio of A_n to leaf transpiration) can be expressed simply, in the case of a zero value of g_c:

$$W_{UE} = \frac{C_s - \Gamma}{1.6\rho_a}\left[\frac{f_0^*}{D^*_{\max}} + \frac{1 - f_0^*}{D_s}\right]. \quad \text{(A7)}$$

where ρ_a is air density.

[52] The influence of soil moisture stress on g_m, f_0 and $D_{\max}$ is described by *Calvet* [2000] and *Calvet et al.* [2004].

[53] The PAR extinction by the canopy must be described in the model: the leaves on top of the canopy intercept a large fraction of the incoming solar radiation, thus reducing the photosynthetic activity of lower layers. Assuming an homogeneous leaf vertical distribution, the integrated canopy net assimilation A_{nI} and conductance g_{sI} can be written as

$$A_{nI} = LAI \int_0^1 A_n d(z/h) \quad \text{(A8)}$$

and

$$g_{sI} = LAI \int_0^1 g_s d(z/h), \quad \text{(A9)}$$

where h is canopy height and z is the distance to the ground (see *Calvet et al.* [1998] for further details).

Appendix B: Growth Model

[54] The leaf area index LAI is derived from the leaf biomass B, related to the net assimilation of the canopy A_{nI} (equation (A8), expressed in units of $kgCO_2\ m^{-2}\ s^{-1}$): growth is described as the accumulation of carbon obtained from assimilation of atmospheric CO_2, and senescence as the result of a deficit of photosynthesis (due to external factors). In ISBA-A-gs, the leaf biomass B is obtained from the differential equation:

$$dB = \frac{M_C}{P_C M_{CO_2}} A_{nI} dt - B\, d(t/\tau), \quad \text{(B1)}$$

where P_C is the proportion of carbon in the dry plant biomass, and M_C and M_{CO2} are the molecular weights of carbon and CO_2, respectively.

[55] The mortality increment term of equation (B1) represents an exponential extinction of B characterized by a time-dependent effective life expectancy (expressed in units of days):

$$\tau(t) = \tau_M \frac{A_{nfm}(t)}{A_{n,\max}}, \quad \text{(B2)}$$

where τ_M is the maximum effective life expectancy of the active biomass, $A_{nfm}(t)$ is the maximum leaf net assimilation reached on the day before time t and $A_{n,\max}$ is the optimum leaf net assimilation [*Calvet et al.*, 1998].

[56] The value of LAI is obtained from B by:

$$LAI = B/\alpha_B. \quad \text{(B3)}$$

[57] The definition of the α_B ratio was modified in this study (see section 3.1).

[58] The computed value of LAI is related to the integrated net assimilation through the growth model represented by equations (B1) –(B3). Plant growth depends on two parameters, the α_B ratio and τ_M.

[59] In the simple allocation scheme employed in this study, two biomass reservoirs are considered: the leaf biomass (B) and the structural biomass (B_s), forming the total nonwoody aboveground biomass (B_T):

$$B_T = B + B_s. \quad \text{(B4)}$$

[60] In the plant N-decline model, the total nonwoody aboveground biomass is related to the leaf biomass by the following allometric equation [*Calvet and Soussana*, 2001]:

$$B_T = \left(\frac{B}{c}\right)^{1/(1-a)}, \quad \text{(B5)}$$

where c and a are constant parameters (c = 0.754 and a = 0.38).

[61] The B-decline term of equation (B1) is split into a mortality and a storage term (M_B and S_B, respectively):

$$B\, d(t/\tau) = M_B + S_B. \quad \text{(B6)}$$

[62] The way the distinction is made between M_B and S_B is described below. The growing phase is characterized by positive values of dB in equation (B1), when net assimilation exceeds the B-decline term. When this condition is satisfied, the plant N decline model can be applied: the aboveground biomass B_T is derived from B using equation (B5) and B_s is the difference between the two terms (equation (B4)). The mortality of B_s is given by:

$$M_{Bs} = B_s\, d(t/\tau_M). \quad \text{(B7)}$$

[63] The structural biomass also loses carbon through respiration:

$$R_{Bs} = \eta_R B_S Q_{10}^{(T-25)/10} dt, \quad \text{(B8)}$$

where dt represents one day, T is surface temperature (in °C), η_R a respiration coefficient of 1% of B_s per day, and $Q_{10} = 2$.

[64] Finally, the storage term S_B of equation (B6) is calculated as the residual of the structural biomass budget:

$$S_B = dB_s + M_{Bs} + R_{Bs}. \tag{B9}$$

[65] The M_B term of equation (B6) is obtained by difference. In situations where storage exceeds the mortality of active biomass M_B, an alternative formulation of B-decline is employed. B_T is recalculated assuming that there is no loss of leaf biomass outside the plant system, during the considered time step: $M_B = 0$ and dB_T is the difference between the daily net assimilation and the mortality and respiration losses of structural biomass (equations (B7) and (B8)). The leaf biomass B is derived from B_T using equation (B5), and B_s is the difference between the two terms (equation (B4)). A new value of the storage term S_B is given by equation (B9).

[66] When the vegetation becomes senescent (negative values of dB), the plant N decline equation (equation (B5)) is no longer valid. In this case, the B_s reservoir evolves independently from B: a nil storage term is prescribed and the mortality and respiration losses (equations (B7) and (B8)) are applied to B_s.

Appendix C: Relationships Between g_m^*, f_o^* and D_{max}^*

[67] For herbaceous species, *Calvet* [2000] found interspecific and intraspecific relationships between optimized values of g_m^* and D_{max}^*:

$$\begin{aligned} \ln(g_m^*) &= 2.381 - 0.6103 \ln(D_{max}^*) \text{ for } C_3 \text{ plants,} \\ \ln(g_m^*) &= 5.323 - 0.8929 \ln(D_{max}^*) \text{ for } C_4 \text{ plants,} \end{aligned} \tag{C1}$$

with g_m^* in mm s^{-1} and D_{max}^* in g kg^{-1}.

[68] f_o^* was set to constant values:

$$\begin{aligned} f_0^* &= 0.95 \text{ for } C_3 \text{ plants,} \\ f_0^* &= 0.6, \text{ for } C_4 \text{ plants.} \end{aligned} \tag{C2}$$

[69] For woody species, *Calvet et al.* [2004] determined the following relationship between g_m^* and f_o^*:

$$\ln(g_m^*) = 4.7 - 7 f_0^*, \tag{C3}$$

with g_m^* in mm s^{-1}.

[70] **Acknowledgments.** The authors wish to thank the GSWP-2, ISLSCP-II, MODIS and ECOCLIMAP teams for providing the data sets. This study was cofunded by the European Commission within the GMES initiative in FP6, in the framework of the geoland integrated GMES project on land cover and vegetation.

References

Arora, V. K. (2002), Modeling vegetation as a dynamic component in soil-vegetation-atmosphere transfer schemes and hydrological models, *Rev. Geophys.*, *40*(2), 1006, doi:10.1029/2001RG000103.

Arora, V. K., and G. K. Boer (2005), A parameterization of leaf phenology for the terrestrial ecosystem component of climate models, *Global Change Biol.*, *11*, 39–59, doi:10.1111/j.1365-2486.2004.00890.x.

Asner, G. P., J. M. O. Scurlock, and J. A. Hicke (2003), Global synthesis of leaf area index observations: Implications for ecological and remote sensing studies, *Global Ecol. Biogeogr.*, *12*, 191–205.

Betts, R. A., P. M. Cox, S. E. Lee, and F. I. Woodward (1997), Contrasting physiological and structural vegetation feedbacks in climate change simulations, *Nature*, *387*, 796–799.

Bondeau, A., D. W. Kicklighter, J. Kaduk, and the Participants of the Postdam NPP Model Intercomparison (1999), Comparing global models of terrestrial net primary productivity (NPP): Importance of vegetation structure on seasonal NPP estimates, *Global Change Biol.*, *5*, 35–45.

Botta, A., N. Viovy, P. Ciais, P. Friedlinstein, and P. Monfray (2000), A global prognostic scheme of leaf onset using satellite data, *Global Change Biol.*, *6*, 709–725.

Bounoua, L., et al. (1999), Interactions between vegetation and climate: Radiative and physiological effects of doubled atmospheric CO_2, *J. Clim.*, *12*, 309–324.

Buermann, W., Y. Wang, J. Dong, L. Zhou, X. Zeng, R. E. Dickinson, C. S. Potter, and R. B. Myneni (2002), Analysis of a multiyear global vegetation leaf area index data set, *J. Geophys. Res.*, *107*(D22), 4646, doi:10.1029/2001JD000975.

Calvet, J.-C. (2000), Investigating soil and atmospheric plant water stress using physiological and micrometeorological data, *Agric. For. Meteorol.*, *103*, 229–247.

Calvet, J.-C., and J.-F. Soussana (2001), Modelling CO_2-enrichment effects using an interactive vegetation SVAT scheme, *Agric. For. Meteorol.*, *108*, 129–152.

Calvet, J.-C., J. Noilhan, J.-L. Roujean, P. Bessemoulin, M. Cabelguenne, A. Olioso, and J.-P. Wigneron (1998), An interactive vegetation SVAT model tested against date from six contrasting sites, *Agric. For. Meteorol.*, *92*, 73–95.

Calvet, J.-C., V. Rivalland, C. Picon-Cochard, and J.-M. Guehl (2004), Modelling forest transpiration and CO_2 fluxes - Response to soil moisture stress, *Agric. For. Meteorol.*, *124*, 143–156.

Ciais, P., P. P. Tans, and M. Trolier (1995), A large northern-hemisphere terrestrial CO_2 sink indicated by the $^{13}C/^{12}C$ ratio of atmospheric CO_2, *Science*, *209*, 1098–1102.

Cox, P. M., C. Huntingford, and R. J. Harding (1998), A canopy conductance and photosynthesis model for use in a GCM land surface scheme, *J. Hydrol.*, *212–213*, 79–94.

Cox, P. M., R. A. Betts, C. D. Jones, S. A. Spall, and I. J. Totterdell (2000), Acceleration of global warming due to carbon-cycle feedbacks in a coupled climate model, *Nature*, *408*, 184–187.

Dan, L., J. Ji, and Y. Li (2005), Climatic and biological simulations in a two-way coupled atmosphere-biosphere model, *Global Planet. Change*, *47*, 153–169.

Decharme, B., and H. Douville (2005), Uncertainties in the GSWP-2 precipitation forcing and their impacts on regional and global hydrological simulations, *Clim. Dyn.*, doi:10.1007/s00382-006-0160-6, in press.

Déqué, M., C. Dreveton, A. Braun, and D. Cariolle (1994), The ARPEGE/IFS atmosphere model, A contribution to the French community climate modelling, *Clim. Dyn.*, *10*, 249–266.

Dickinson, R. E., M. Shaikh, R. Bryant, and L. Graumlich (1998), Interactive canopies for a climate model, *J. Clim.*, *11*, 2823–2836.

Dirmeyer, P. A., A. J. Dolman, and N. Sato (1999), The Global Soil Wetness Project: A pilot project for global land surface modeling and validation, *Bull. Am. Meteorol. Soc.*, *80*, 851–878.

Dirmeyer, P. A., X. Gao, and T. Oki (2002), The Second Global Soil Wetness Project GSWP2: Science and implementation plan, *IGPO Publ. 37*, Int. GEWEX Proj. Off., Washington, D. C.

Dirmeyer, P. A., X. Gao, M. Zhao, Z. Guo, T. Oki, and N. Hanasaki (2005), The Second Global Soil Wetness Project GSWP2: Multi-model analysis and implications for our perception of the land surface, *COLA Tech. Rep. 185*, Cent. for Ocean-Land-Atmos. Stud., Calverton, Md.

Douville, H., S. Planton, J.-F. Royer, D. Stephenson, S. Tyteca, L. Kergoat, S. Lafont, and R. Betts (2000), Importance of vegetation feedbacks in doubled-CO_2 climate experiments, *J. Geophys. Res.*, *105*, 14,841–14,861.

Foley, J. A., I. C. Prentice, N. Ramunkutty, S. Levis, D. Pollard, S. Sitch, and A. Haxeltine (1996), An integrated biosphere model of land surface processes, terrestrial carbon balance, and vegetation dynamics, *Global Biogeochem. Cycles*, *10*, 603–628.

Friedl, M. A., et al. (2002), Global land cover mapping from MODIS: Algorithms and early results, *Remote Sens. Environ.*, *83*, 287–302.

Gibelin, A.-L., and M. Déqué (2003), Anthropogenic climate change over the Mediterranean region simulated by a global variable resolution model, *Clim. Dyn.*, *20*, 327–339.

Gong, D. Y., and P. J. Shi (2003), Northern hemispheric NDVI variations associated with large-scale climate indeices in spring, *Int. J. Remote Sens.*, *12*, 2559–2566.

Hall, F. G., G. Collatz, Los, S. O., E. Brown de Colstoun, and D. Landis (Eds.) (2005), *ISLSCP Initiative II*, NASA, DVD/CD-ROM.

Houghton, J., , Y. Ding, D. Griggs, M. Noguer, P. van der Linden, X. Dai, K. Maskell, and C. Johnson (Eds.) (2001), *Climate Change 2001: The Scientific Basis. Contribution of Working Group I to the Third Assesment Report of the Intergovernmental Panel on Climate Change*, Cambridge Univ. Press, New York.

Jacobs, C. M. J., B. J. J. M. van den Hurk, and H. A. R. de Bruin (1996), Stomatal behaviour and photosynthetic rate of unstressed grapevines in semi-arid conditions, *Agric. For. Meteorol.*, *80*, 111–134.

Jarvis, P. G. (1976), The interpretation of the variations in leaf water potential and stomatal conductance found in canopies in the field, *Philos. Trans. R. Soc. London, Ser. B*, *273*, 593–610.

Jolly, W. M., R. Nemani, and S. W. Running (2005), A generalized, bioclimatic index to predict foliar phenology in response to climate, *Global Change Biol.*, *11*, 619–632, doi:10.1111/j.1365-2486.2005.00930.x.

Jonckheere, I., S. Fleck, K. Nackaerts, B. Muys, P. Coppin, M. Weiss, and F. Baret (2004), Review of methods for in situ leaf area index determination Part Theories, I., sensors and hemispherical photography, *Agric. For. Meteorol.*, *121*, 19–35, doi:10.1016/j.agrformet.2003.08.027.

Justice, C. O., G. Townshend, E. F. Vermotte, E. Masuoka, R. E. Wolfe, N. Saleous, D. P. Roy, and J. T. Morisette (2002), An overview of MODIS Land data processing and product status, *Remote Sens. Environ.*, *83*, 3–15.

Keeling, R., S. Piper, and M. Heimann (1996), Global and hemispheric carbon dioxide sinks deduced from changes in atmospheric O_2 concentration, *Nature*, *381*, 218–221.

Kergoat, L., S. Lafont, H. Douville, B. Berthelot, G. Dedieu, S. Planton, and J.-F. Royer (2002), Impact of doubled CO_2 on global scale leaf area index and evapotranspiration: Conflicting stomatal and LAI responses, *J. Geophys. Res.*, *107*(D24), 4808, doi:10.1029/2001JD001245.

Knyazikhin, Y., J. V. Martonchik, R. B. Myneni, D. J. Diner, and S. W. Running (1998), Synergistic algorithm for estimating vegetation canopy leaf area index and fraction of absorbed photosynthetically active radiation from MODIS and MISR data, *J. Geophys. Res.*, *103*, 32,257–32,276.

Körner, C. (2000), Biosphere responses to CO_2 enrichment, *Ecol. Appl.*, *10*, 1590–1619.

Körner, C. (2003), Ecological impacts of atmospheric CO_2 enrichment on terrestrial ecosystems, *Philos. Trans. R. Soc. London, Ser. A*, *361*, 2023–2041.

Krinner, G., N. Viovy, N. de Noblet-Ducoudré, J. Ogée, J. Polcher, P. Friedlingstein, P. Ciais, S. Sitch, and I. Prentice (2005), A dynamic global vegetation model for studies of the coupled atmosphere-biosphere system, *Global Biogeochem. Cycles*, *19*, GB1015, doi:10.1029/2003GB002199.

Los, S. O., et al. (2000), A global 9–year biophysical land surface dataset from NOAA AVHRR data, *J. Hydrometeorol.*, *1*, 183–199.

Los, S. O., P. R. J. North, W. M. F. Grey, and M. J. Barnsley (2005), A method to convert AVHRR Normalized Difference Index time series to a standard viewing and illumination geometry, *Remote Sens. Environ.*, *99*, 400–411, doi:10.1016/j.rse.2005.08.017.

Masson, V., J.-L. Champeaux, F. Chauvin, C. Meriguet, and R. Lacaze (2003), A global database of land surface parameters at 1–km resolution in meteorological and climate models, *J. Clim.*, *16*, 1261–1282.

Moulin, S., L. Kergoat, N. Viovy, and G. Dedieu (1997), Global-scale assessment of vegetation phenology using NOAA/AVHRR satellite measurements, *J. Clim.*, *10*, 1154–1170.

Myneni, R. B., C. D. Keeling, C. J. Tucker, G. Asrar, and R. R. Nemani (1997), Increased plant growth in the northern high latitudes from 1981 to 1991, *Nature*, *386*, 698–702.

Myneni, R. B., et al. (2002), Global products of vegetation leaf area and fraction absorbed PAR from year one of MODIS data, *Remote Sens. Environ.*, *83*, 214–231.

Nemani, R. R., C. D. Keeling, H. Hashimoto, W. M. Jolly, S. C. Piper, C. J. Tucker, R. B. Myneni, and S. W. Running (2003), Climate-driven increases in global terrestrial net primary production from 1982 to 1999, *Science*, *300*, 1560–1563.

Noilhan, J., and J.-F. Mahfouf (1996), The ISBA land surface parameterisation scheme, *Global Planet. Change*, *13*, 145–159.

Noilhan, J., and S. Planton (1989), A simple parameterization of land surface processes for meteorological models, *Mon. Weather Rev.*, *117*, 536–549.

Pielke, R. A., R. Avissar, M. Raupach, A. J. Dolman, X. Zeng, and A. S. Denning (1998), Interactions between the atmosphere and terrestrial ecosystems: Influence on weather and climate, *Global Change Biol.*, *4*, 461–475.

Pitman, A. J. (2003), The evolution of, and revolution in, land surface schemes designed for climate models, *Int. J. Climatol.*, *23*, 479–510.

Poorter, H. (1993), Interspecific variation in the growth response of plants to an elevated ambient CO_2 concentration, *Vegetatio*, *104/105*, 77–97.

Prentice, I., et al. (2001), The carbon cycle and atmospheric CO_2, in *Climate Change 2001: The Scientific Basis: Contribution of WGI to the Third Assessment Report of the IPCC*, pp. 183–237, Cambridge Univ. Press, New York.

Reich, P. B., and J. Oleksyn (2004), Global patterns of plant leaf N and P in relation to temperature and latitude, *Proc. Natl. Acad. Sci. U. S. A.*, *101*, 11,001–11,006.

Reich, P. B., D. S. Ellsworth, M. B. Walters, J. M. Vose, C. Gresham, J. C. Volin, and W. D. Bowman (1999), Generality of leaf trait relationships: A test across six biomes, *Ecology*, *80*, 1955–1969.

Richard, Y., and I. Poccard (1998), A statistical study of NDVI sensitivity to seasonal and interannual rainfall variations in Southern Africa, *Int. J. Remote Sens.*, *15*, 2907–2920.

Rivalland, V. (2003), Amélioration et validation du modèle de fonctionnement de la végétation ISBA-A-gs: Stress hydrique et flux de CO_2, Ph.D. thesis, Univ. Paul Sabatier, Toulouse.

Rivalland, V., J.-C. Calvet, P. Berbigier, Y. Brunet, and A. Granier (2005), Transpiration and CO_2 fluxes of a pine forest: Modelling the undergrowth effect, *Ann. Geophys.*, *23*, 1–14.

Roujean, J.-L., and R. Lacaze (2002), Global mapping of vegetation parameters from POLDER multi-angular measurements for studies of surface-atmosphere interactions: A pragmatic method and its validation, *J. Geophys. Res.*, *107*(D12), 4150, doi:10.1029/2001JD000751.

Schulze, E. D., F. M. Kelliher, C. Körner, J. Lloyd, and R. Leuning (1994), Relationships among maximum stomatal conductance, ecosystem surface conductance, carbon assimilation rate, and plant nitrogen nutrition: A global ecology scaling exercise, *Annu. Rev. Ecol. Syst.*, *25*, 629–660.

Sellers, P. J., D. A. Randall, G. J. Collatz, J. A. Berry, C. B. Field, D. A. Dazlich, C. Zhang, G. D. Collelo, and L. Bounoua (1996a), A revised land surface parameterization (SiB2) for atmospheric GCMs. Part I: Model formulation, *J. Clim.*, *9*, 676–705.

Sellers, P. J., et al. (1996b), Comparison of radiative and physiological effects of doubled atmospheric CO_2 on climate, *Science*, *271*, 1402–1406.

Sellers, P. J., et al. (1997), Modeling the exchanges of energy, water, and carbon between continents and the atmosphere, *Science*, *275*, 502–509.

Tanaka, K., K. Yorozu, R. Hamabe, and S. Ikebuchi (2004), Validation of the GSWP2 baseline simulation, paper presented at 85th Annual Meeting - 19th Conference on Hydrology, Am. Meteorol. Soc., San Diego, Calif.

Voirin, S., J.-C. Calvet, F. Habets, and J. Noilhan (2001), Interactive vegetation modelling at a regional scale: Application to the Adour basin, *Plant Cell Environ.*, *26*, 479–484.

Wang, Q., J. Tenhunen, N. Q. Dinh, M. Reichstein, D. Otieno, A. Granier, and K. Pilegarrd (2005), Evaluation of seasonal variation of MODIS derived leaf area index at two European deciduous broadleaf forest sites, *Remote Sens. Environ.*, *96*, 475–484.

White, M. A., P. E. Thornton, and S. W. Running (1997), A continental phenology model for monitoring vegetation responses to interannual climatic variability, *Global Biogeochem. Cycles*, *11*, 217–234.

Zeng, N., J. D. Neelin, K. M. Lau, and C. J. Tucker (1999), Enhancement of interdecadal climate variability in the Sahel by vegetation interaction, *Science*, *286*, 1537–1540.

Zhao, M., and P. A. Dirmeyer (2003), Production and analysis of GSWP-2 near surface meteorology data sets, *COLA Tech. Rep. 159*, Cent. for Ocean-Land-Atmos. Stud., Calverton, Md.

Zhou, L., C. J. Tucker, R. K. Kaufmann, D. Slayback, N. V. Shabanov, and R. B. Myneni (2001), Variations in northern vegetation activity inferred from satellite data of vegetation index during 1981 to 1999, *J. Geophys. Res.*, *106*, 20,069–20,083.

Zhou, L., R. K. Kaufmann, Y. Tian, R. B. Myneni, and C. J. Tucker (2003), Relation between interannual variations in satellite measures of northern forest greeness and climate between 1982 and 1999, *J. Geophys. Res.*, *108*(D1), 4004, doi:10.1029/2002JD002510.

J.-C. Calvet, A.-L. Gibelin, L. Jarlan, and J.-L. Roujean, Groupe d'Etude de l'Atmosphère Météorologique, Météo-France/Centre National de Recherches Météorologiques, 42, Avenue Coriolis, F-31057 Toulouse Cedex 1, France. (anne-laure.gibelin@meteo.fr)

S. O. Los, Department of Geography, University of Wales, Swansea SA2 8PP, UK.